

Rainfall Simulation Associated with Typhoon Herb (1996) near Taiwan. Part I: The Topographic Effect

CHUN-CHIEH WU AND TZU-HSIUNG YEN

Department of Atmospheric Sciences, National Taiwan University, Taipei, Taiwan

YING-HWA KUO AND WEI WANG

National Center for Atmospheric Research, Boulder, Colorado*

(Manuscript received 11 October 2001, in final form 17 June 2002)

ABSTRACT

In this study, a series of numerical experiments are performed to examine the ability of a high-resolution mesoscale model to predict the track, intensity change, and detailed mesoscale precipitation distributions associated with Typhoon Herb (1996), which made landfall over Taiwan. The fifth-generation Pennsylvania State University–National Center for Atmospheric Research Mesoscale Model (MM5), with a 2.2-km horizontal grid spacing, successfully simulates the mesoscale rainfall distribution associated with Herb, and the predicted maximum 24-h rainfall of 1199 mm accounts for about 70% of the observed amount of 1736 mm at Mount A-Li. It is shown that, with an accurate track simulation, the ability of the model to simulate successfully the observed rainfall is dependent on two factors: the model's horizontal grid spacing and its ability to describe the Taiwan terrain. The existence of the Central Mountain Range has only a minor impact on the storm track, but it plays a key role in substantially increasing the total rainfall amounts over Taiwan. The analysis presented here shows that the model and terrain resolutions play a nearly equivalent role in the heavy precipitation over Mount A-Li. The presence of maximum vertical motion and heating rate in the lower troposphere, above the upslope mountainous region, is a significant feature of forced lifting associated with the interaction of the typhoon's circulation and Taiwan's mountainous terrain. Overall, Typhoon Herb is a case in point to indicate the intimate relation between Taiwan's topography and the rainfall distribution associated with a typhoon at landfall.

1. Introduction

Typhoon Herb (1996) made landfall at I-Lan in northeastern Taiwan at 1444 UTC 31 July 1996 and was one of the most damaging tropical cyclones in the recent history of Taiwan (Wu and Kuo 1999). Besides the intense, gusty winds associated with Typhoon Herb (maximum sustained surface winds of 65 m s^{-1} were recorded), the most interesting aspect of the storm was the torrential rainfall it produced over the Central Mountain Range (CMR). As Typhoon Herb traversed northern Taiwan, the airflow over the main body of Taiwan changed from northwesterly to westerly and then to southwesterly (Shieh et al. 1997), bringing the moisture-laden typhoon circulation over the CMR. The lifting associated with this upslope motion generated extremely

heavy precipitation over central Taiwan, which caused, in turn, many landslides and debris flows, as well as heavy losses of life and property.

Figure 1a shows the observed rainfall accumulations during the passage of Herb from 0000 UTC 31 July to 0000 UTC 1 August and shows the corresponding Taiwan terrain. Two major precipitation centers are identified: one at Mount Nio-Dray in northern Taiwan, with a maximum total precipitation of 858 mm, and the other at Mount A-Li in central Taiwan, with a record-breaking total accumulation of 1736 mm over the 1-day period. In sharp contrast, downslope flow persisted over eastern Taiwan, and very little precipitation was recorded. The downslope flow also created a topography-induced mesoscale pressure area over eastern Taiwan between Hualien and Taitung.

The track of Herb is simulated well by most dynamic and statistical models (Wu and Kuo 1999). It has been shown (Wang 1980, 1989) that the mesoscale precipitation distributions associated with typhoons near Taiwan are highly modulated by the topography of Taiwan. Therefore, the statistical and analog methods may provide a reasonable rainfall forecast as long as the typhoon track is predicted well. However, a more challenging

* The National Center for Atmospheric Research is sponsored by the National Science Foundation.

Corresponding author address: Dr. Chun-Chieh Wu, Dept. of Atmospheric Sciences, National Taiwan University, 61, Ln. 144, Sec. 4, Keelung Rd., Taipei 10772, Taiwan.
E-mail: cwu@typhoon.as.ntu.edu.tw

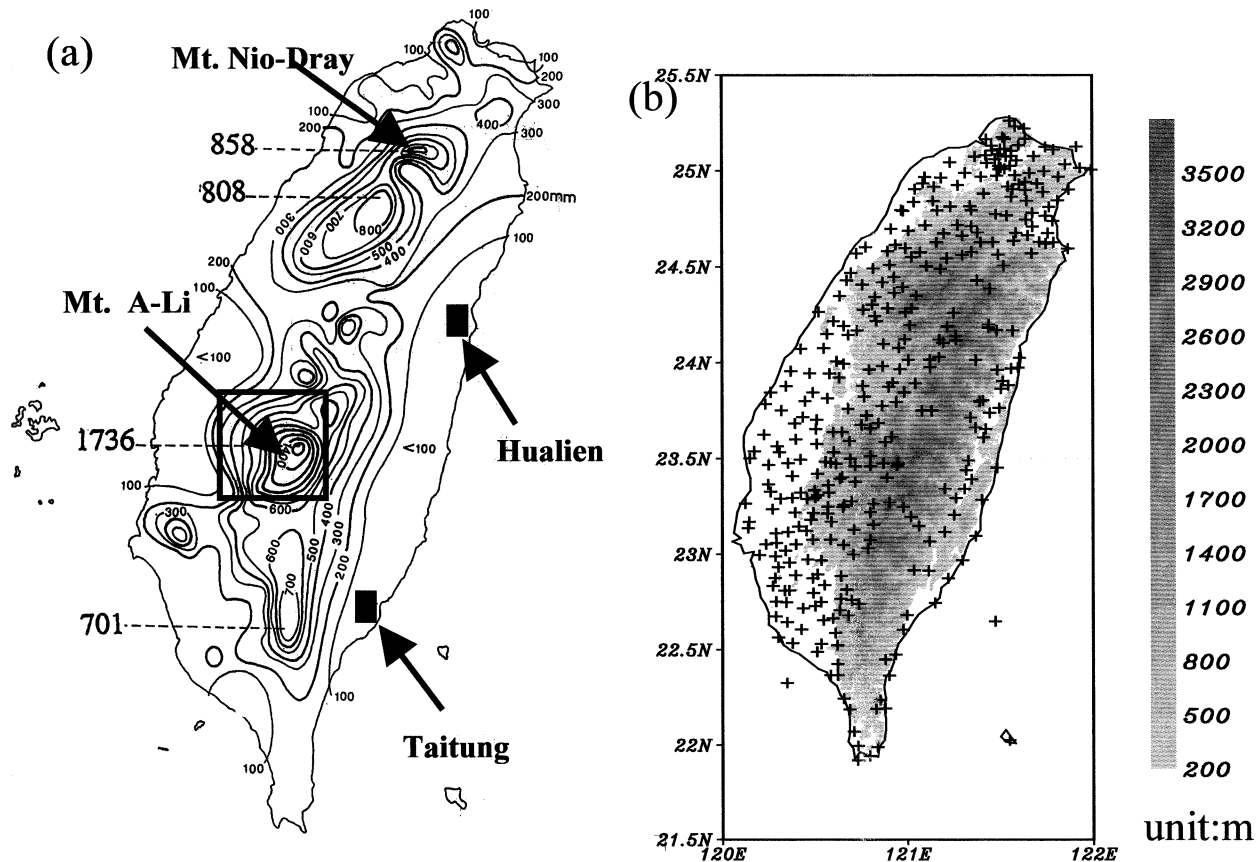


FIG. 1. (a) The 24-h (0000 UTC 31 Jul–0000 UTC 1 Aug 1996) accumulated rainfall (contour interval of 100 mm) during passage of Typhoon Herb (after Shieh et al. 1997). The thickened square box indicates the region (23.3° – 23.7° N, 120.6° – 121.0° E) for the area average used in Figs. 12, 13, and 15 and Tables 2 and 3. Line AB (along 23.3° N, and from 120° to 122° E) is used for cross-sectional analyses in Figs. 7 and 9. (b) Taiwan terrain shown in shading. The plus signs indicate the locations of the 327 rain gauge stations whose rainfall data are used to plot the rainfall distribution in (a).

scientific, as well as forecasting, question is the following: Given good track prediction, can a numerical model provide a good rainfall forecast for a landfalling typhoon of the intensity approximate to Herb's? If it can, what are the key elements affecting rainfall prediction? To answer the above questions, following the preliminary analysis of Kuo and Wang (1997) and Wu and Kuo (1999), we use a high-resolution numerical model with detailed topography of the CMR to study the physical mechanisms that affected the mesoscale precipitation distribution as Herb approached and crossed northern Taiwan. Results obtained from this study can also shed light on important scientific issues related to (a) hurricanes at landfall and (b) quantitative precipitation forecasts, both of which are the foci of the U.S. Weather Research Program (Emanuel et al. 1995; Marks et al. 1998).

Considerable progress has been made over the past 10 years in the prediction of tropical cyclone track with a numerical model (Kurihara et al. 1995, 1998). Recent work (e.g., Liu et al. 1997, 1999) has also successfully demonstrated the capability of high-resolution nonhy-

drostatic mesoscale models in realistically simulating the detailed mesoscale structure of a hurricane. As an example, Farfan and Zehnder (2001) successfully simulated the track and storm structure of Hurricane Nora's (1997) interaction with the Baja California Peninsula, using a version of the fifth-generation Pennsylvania State University–National Center for Atmospheric Research Mesoscale Model (MM5). Meanwhile, Wang (2001) demonstrated that a high-resolution model has the capability of simulating many aspects of tropical cyclones, including the inner core structure, the inner and outer spiral rainbands, and the vortex Rossby waves within the rotating eyewall. Following Kuo and Wang (1997), in this work, we experiment with a high-resolution (2.2 km grid spacing) MM5 configuration to simulate Typhoon Herb. Our primary objective is to investigate the ability of the model to simulate the track, intensity, and detailed precipitation distribution associated with Typhoon Herb. In particular, we assess the effect of the model resolution and detailed topography on rainfall simulation. The model description and experiment design are presented in section 2. Section 3

TABLE 1. Summary of numerical experiments [BM is Betts and Miller (1986)].

Expt	Cumulus parameterization scheme	Horizontal grid spacing (km)	Model topography resolution (km)	Bogusing	Environmental flow
E60	BM	60	60	Yes	
E20	BM	20	20	Yes	
E6.7	None	6.7	6.7	Yes	Environmental flow field based on Kurihara et al. (1995)
E2.2	None	2.2	2.2	Yes	
E6.7/NB	None	6.7	6.7	None	
E6.7/NT	None	6.7	None	Yes	
E6.7/20	None	6.7	20	Yes	
E2.2/6.7	None	2.2	6.7	Yes	

provides the results of the model simulations. The summary is provided in section 4.

2. Model description and experiment design

This study makes use of MM5 (Dudhia 1993; Grell et al. 1994), which is a nonhydrostatic, primitive equation model in sigma coordinates. A suite of model physical parameterization schemes is available for subgrid-scale convection, grid-resolvable scale, microphysical parameterization, planetary boundary layer (PBL) physics, and radiation. The particular version of MM5 used in the control experiment includes the following physics options: 1) the Betts and Miller (1986) cumulus parameterization, 2) the Blackadar PBL scheme, 3) the atmospheric radiation scheme of Dudhia (1989), and 4) the Reisner mixed-phase microphysics without graupel (Reisner et al. 1998).

The initial and lateral boundary conditions are based on the European Centre for Medium-Range Weather Forecasts (ECMWF)/Tropical Ocean–Global Atmosphere (EC/TOGA) global analysis, with the fixed sea surface temperature (SST) data taken from the weekly mean SST available at the National Centers for Environmental Prediction. The model initialization is performed as follows (also see Wu and Huang 2000): we first perform a doubly nested 60-/20-km MM5 simu-

lation, starting at 1200 UTC 29 July, with a bogus Rankine vortex derived from the characteristics of the storm and estimated by the best-track analysis. As the typhoon vortex becomes well developed at 12 h (0000 UTC 30 July), with an intensity (i.e., minimum central sea level pressure of 930 hPa) identical to the analyzed value from the Joint Typhoon Warning Center (JTWC), the 700-km-radius inner circular area of the fully developed, asymmetric, typhoon vortex, which matches the estimated storm size, is lifted from the model simulation to merge smoothly with the environmental flow field, which has been derived from EC/TOGA analysis at 0000 30 July [using the filtering method from Kurihara et al. (1995)]. The spunup typhoon vortex is placed at the observed storm location, according to the best-track analysis. The forward model simulation then commences at 0000 UTC 30 July and is integrated for 48 h, ending at 0000 UTC 1 August.

To improve our understanding of the physical processes affecting the behavior of the rainfall simulation, a series of experiments with different horizontal resolutions and topographies have been conducted (see Table 1). First, we perform a set of control experiments with 23 fixed vertical levels in sigma coordinate, yet with different horizontal resolutions. These experiments use the before-mentioned PBL, radiation, and cumulus parameterization schemes. Note that the cumulus parameterization schemes are turned off for simulations with horizontal grid spacings of 6.7 km or higher, which will be discussed later. Experiment E60 is a single-mesh experiment with a horizontal resolution of 60 km. E20 is the control experiment with the two-way nested 60-/20-km meshes, which allows feedback between the inner and outer nests. Experiment E6.7 (E2.2) is a single-mesh simulation, with a horizontal spacing of 6.7 (2.2) km, and is run in one-way mode [i.e., the simulation from E6.7 (E2.2) does not feed back to the simulation in E20 (E6.7)], with initial and boundary conditions provided from the output of E20 (E6.7) (see the configuration of the model nested-grid domains in Fig. 2). With the 2.2-km spacing, the model terrain resolves well the CMR features over central Taiwan, as shown in the comparison of the 30'' Taiwan terrain in Fig. 1b with the model terrain of E2.2 (see Fig. 6d, described later).

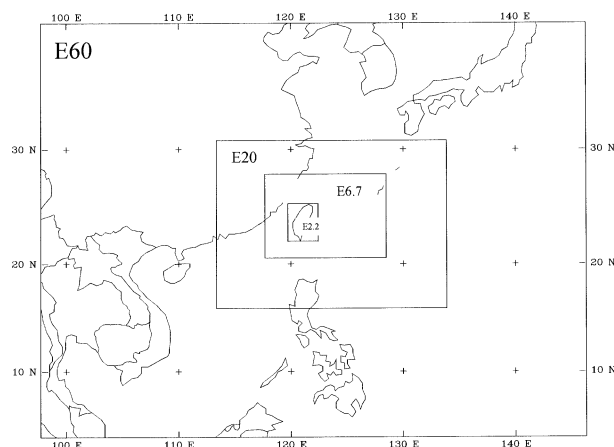


FIG. 2. Configuration of the model nests.

A series of sensitivity experiments (Table 1) are conducted to help to identify the key elements that affect the rainfall simulation of Herb. First, to show the effect of the CMR on the rainfall prediction and wind field distribution, we perform an experiment (E6.7/NT) in which the terrain height of Taiwan in E6.7 is set to zero and is regarded as the ocean surface. Second, to understand the impact of the vortex initialization procedure, an experiment (E6.7/NB) similar to E6.7 is carried out, except that the initial condition is taken directly from the ECMWF global analysis without applying the aforementioned initialization and bogusing procedures. Third, to understand the relative importance of the model resolution and model terrain on the rainfall simulation, we conduct two additional experiments (E6.7/20 and E2.2/6.7) that are identical to E6.7 and E2.2, except their model terrain is obtained from E20 and E6.7, respectively (e.g., in E6.7/20, the model resolution is 6.7 km, yet its terrain is interpolated from the 20-km-based data in E20). Note that the cumulus parameterization scheme is not used for experiments with 6.7-km-or-higher grid spacing. However, we have also carried out a set of experiments with 20-km grid spacing, using different cumulus parameterizations, but we found track and rainfall patterns (figures not shown) similar to those in E20. As a consequence, issues regarding the model's sensitivity to cumulus parameterizations are not discussed in this paper.

3. Results

a. Initialization

Initialization (including bogusing) is an important issue for typhoon simulation (Kurihara et al. 1995). Figure 3 shows the comparison of the east–west cross sections of potential vorticity (PV), horizontal wind, vertical velocity, and relative humidity (RH) fields, cutting through the storm center at 21.2°N and 127.8°E, at the initial time, before, and after the initialization procedures. Before initialization, a broader and weaker storm exists with a maximum horizontal wind of 35 m s⁻¹ at 800 hPa, a maximum PV of 3.4 PVU (potential vorticity unit, 10⁻⁶ m² K s⁻¹ kg⁻¹) at about 450 hPa in the center of the storm (Fig. 3a). After the initialization, high-PV air (Fig. 3b) is concentrated within the inner 200 km of the storm center and extends vertically to about 200 hPa, with a PV maximum of 26 PVU at 250 hPa. The maximum horizontal wind speed (Fig. 3b) reaches 65 m s⁻¹ at 850 hPa, on the eastern flank of the eyewall, with a region of relatively weak wind over the storm center. Although no clear indication of subsidence motion is found in the center, the vertical velocity distribution (Fig. 3b) displays an eyewall-like structure with asymmetric, strong updrafts around the center. To the west of the storm center, an area of strong upward velocity exists, with a maximum value of 202 μb s⁻¹ (roughly equivalent to 2 m s⁻¹) at 450 hPa, which is about 10

times as large as the maximum vertical velocity associated with the storm without initialization (Fig. 3c). The RH distribution (Fig. 3d) indicates the air is totally saturated surrounding the eyewall region but is drier (RH of 60%) within the eye. The above comparison shows that a more realistic storm is obtained after model initialization.

b. Model simulation

1) TRACK AND INTENSITY

Figure 4 shows the comparison of the forecast track of E6.7 with the best-track analyses from JTWC. The MM5 position error, as compared with the JTWC analysis, is 80 and 160 km for the 24- and 48-h forecasts, respectively, and is approximately one-half of the mean track error generated by the operational typhoon prediction models (Wu et al. 2000). In general, all of the control experiments (E60, E20, E6.7, and E2.2) show nearly identical and fairly accurate track simulations for Herb, although the simulated storm moves too fast during the $t = 6$ –12 h periods, resulting in the simulated storm making landfall at 32 h and leaving Taiwan at 38 h, as compared with observed times of 38 and 43 h, respectively.

In the experiment without Taiwan topography (E6.7/NT), the track (Fig. 4) is slightly different from that in E6.7, suggesting a minor track deflection of Herb due to the presence of the CMR. To be specific, the E6.7 track deviates to the right before it approaches the mountain and then deviates to the left as it gets very close to landfall. The storm (E6.7) leaves Taiwan at a latitude slightly south of that of the run without topography (E6.7/NT). The cyclonic turning of the storm's motion is consistent with the findings of Wang (1980), Bender et al. (1987), Yeh and Elsberry (1993a,b), and Wu (2001), although the track deflection is not as significant. This difference is likely attributed to the fact that Herb approaches the lower, northern end of the CMR at a smaller incidence angle (Wang 1980, 1989).

For the intensity simulation, the comparison of the minimum central sea level pressure from the model output (E6.7) with the estimates from JTWC (Fig. 5) indicates that the model intensity agrees well with that from JTWC during most of the integration period. Note that the estimation of the minimum central sea level pressure of Herb remains uncertain, especially over the ocean before landfall, because no in situ observations are available. Although the model simulation has slightly higher pressure by about 5 hPa throughout the forecast period, the model does capture the evolution of Herb's intensity, especially the steadiness and weakening before and during landfall. In general, the overall typhoon structure, as depicted at the initial time in Fig. 3, is maintained well during the first 36-h integration period (figures not shown). In experiment E6.7/NT, the model is able to maintain the storm intensity for a longer

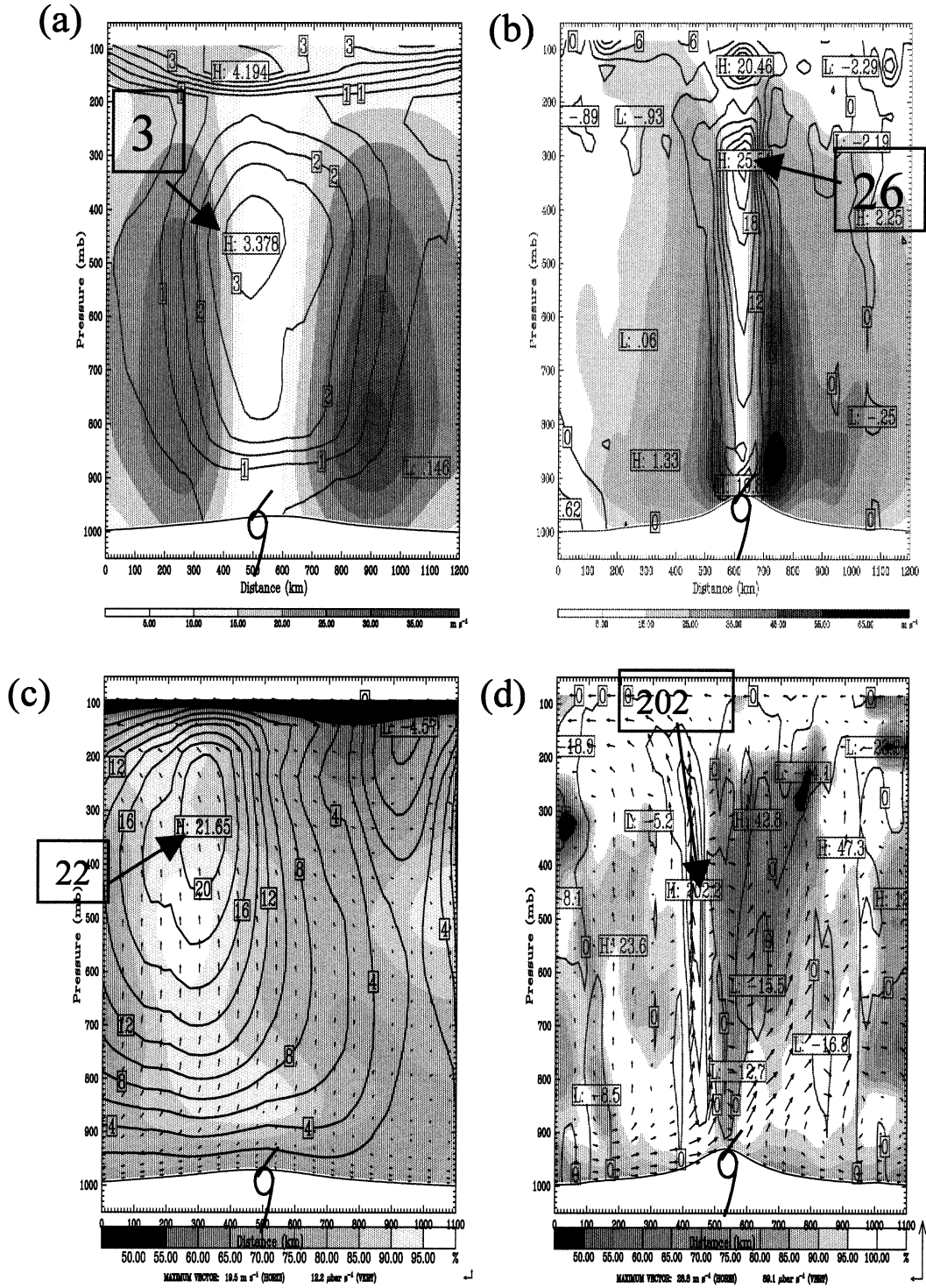


FIG. 3. (a) Zonal cross section of potential vorticity (with contour interval of 3 PVU) and horizontal wind speed (shaded for every 10 $m s^{-1}$) and (c) zonal cross section of vertical motion ($\mu b s^{-1}$) and relative humidity (shaded for every 5%) cutting through the storm center ($21.2^{\circ}N, 127.8^{\circ}E$) at initial time without initialization. (b) and (d) Same as in (a) and (c) but with initialization.

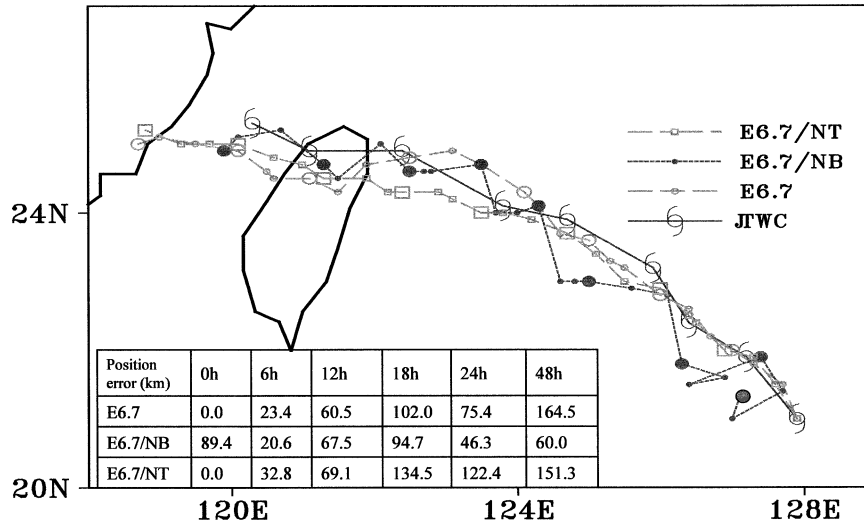


FIG. 4. Tracks of Typhoon Herb (1996) from best tracks of JTWC and from the model experiments. The storm symbol indicates the best track of Herb for every 6 h. The open (solid) circle indicates the model track for expt E6.7 (E6.7/NB) and the square is the model track for expt (E6.7/NT) at 2-h intervals (large symbol for 6-h intervals) from 0000 UTC 30 Jul to 0000 UTC 1 Aug 1996. The position errors (km) are also shown in the attached table.

time period, until it makes landfall near southern China at 40 h.

2) RAINFALL

(i) Control experiments

Figure 6 shows the 24-h accumulated (24–48 h) rainfall prediction and the corresponding model terrain (from 0000 UTC 31 July to 0000 UTC 1 August) from four experiments, with resolutions of 60 (E60), 20 (E20), 6.7 (E6.7), and 2.2 km (E2.2), respectively. Note that, as mentioned above, all four experiments display similar 48-h tracks (figures not shown). Nevertheless, comparison of Figs. 6a and 6b with Fig. 1a clearly indicates that both E60 and E20 produce heavy rainfall

over the western side of the model terrain but underestimate the rainfall amount and cannot simulate the observed mesoscale rainfall distribution. In comparison with the actual Taiwan terrain (Fig. 1b), the model terrains (Figs. 6a,b) in E60 and E20 are too coarse to produce the mesoscale structure of the observed rainfall distribution.

On the other hand, with a finer horizontal grid resolution (Figs. 6c and 6d), the 24-h accumulated rainfall in E6.7 (E2.2) accurately captures the two rainfall maxima: the first over northern Taiwan with a peak amount of 771 (955) mm, the second over Mount A-Li, with a measurement of 826 (1199) mm. The model also predicts a band of precipitation over the southern CMR with an amount exceeding 838 mm for E6.7, which agrees with the observation. Experiment E2.2 overpredicts the rainfall amount, with a measurement of 1286 mm. Meanwhile, the model is successful in capturing the rain shadow over eastern Taiwan, located on the lee side of the mountains. The above results are in agreement with the rainfall pattern over mountainous regions (Lin 1993; Barros and Lettenmaier 1994); that is, local topography enhances strong updraft and intense precipitation on the upwind side of the mountain while the rainfall amount sharply decreases on the lee side.

Besides comparing the simulation of the extreme rainfall, to evaluate the overall performance of the model rainfall, in Fig. 7 we also show the cumulative frequency of the total rainfall based on the data points over the island of Taiwan for each experiment, as well as for the rain gauge observation. The result clearly indicates that the ability of the model to simulate successfully the observed rainfall is degraded by the reduction of the

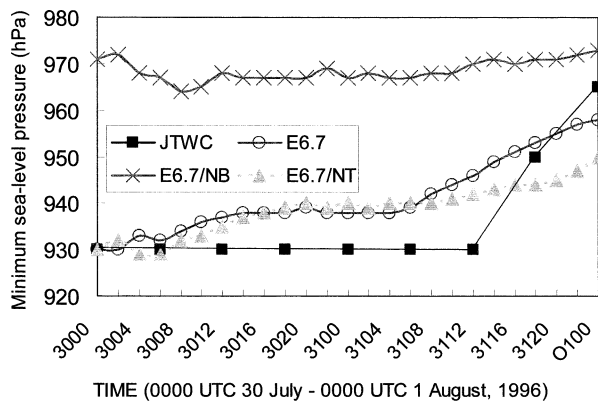


FIG. 5. Time evolution of the central minimum mean sea level pressure of Herb from JTWC (6-h interval) E6.7, E6.7/NB, and E6.7/NT (2-h interval) from 0000 UTC 30 Jul to 0000 UTC 1 Aug 1996.

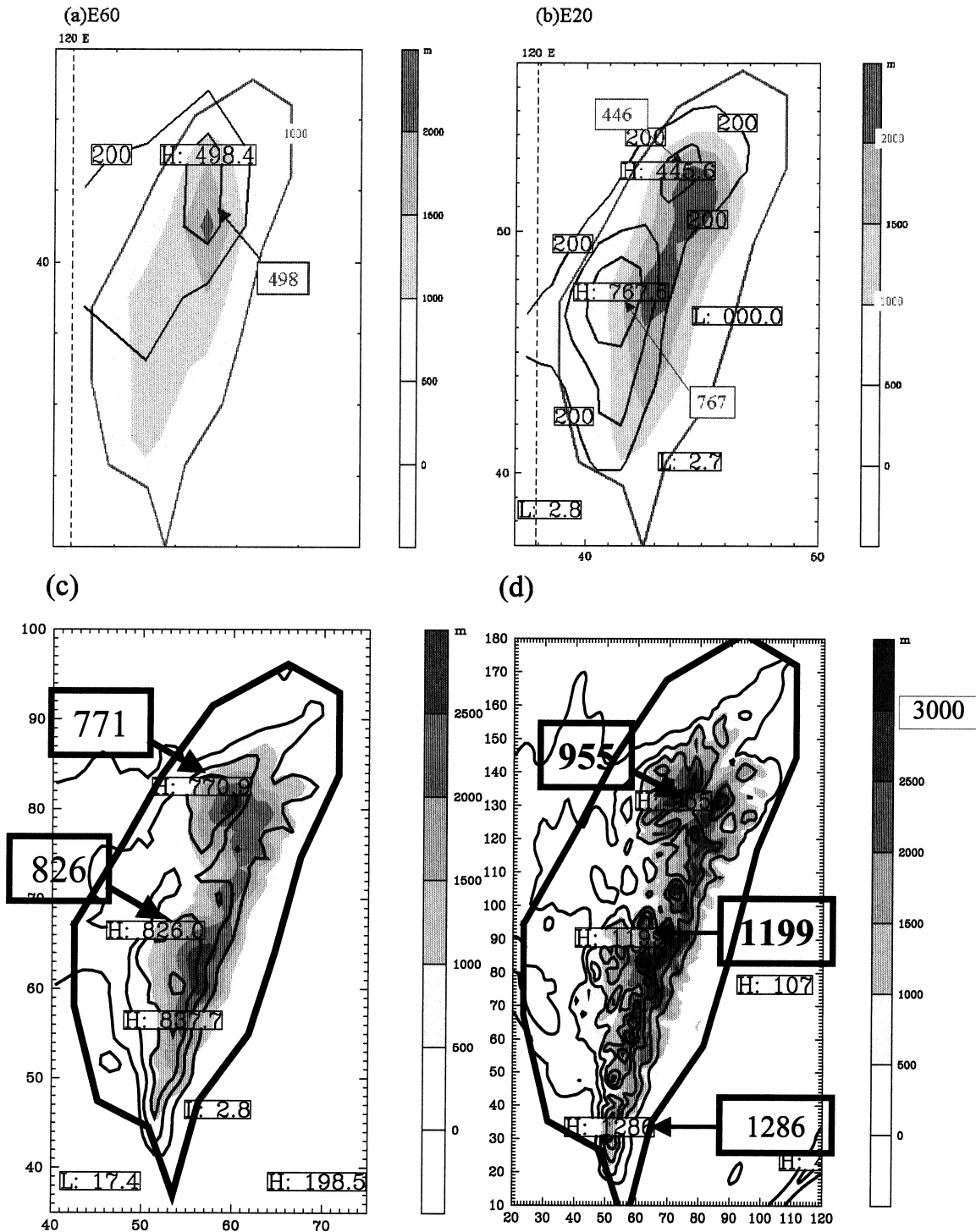


FIG. 6. The 24-h rainfall (with a contour interval of 200 mm) ending at 0000 UTC 1 Aug 1996 from simulations with the highest horizontal grid spacings of (a) 60, (b) 20, (c) 6.7, and (d) 2.2 km. Corresponding model terrains (m) are shown in shading for every 500 m.

horizontal grid resolution. It is interesting to note that the cumulative frequency of E6.7 is much closer to the observations than both E60 and E20 are, and E2.2 nearly matches the observation perfectly. This result implies that, with a horizontal spacing of 2.2 km, the model is

able to pick up the overall rainfall pattern associated with Herb in the Taiwan area. On the other hand, it appears that further increase in the model resolution can hardly improve such a rainfall simulation in E2.2. Therefore, the above results suggest the horizontal spac-

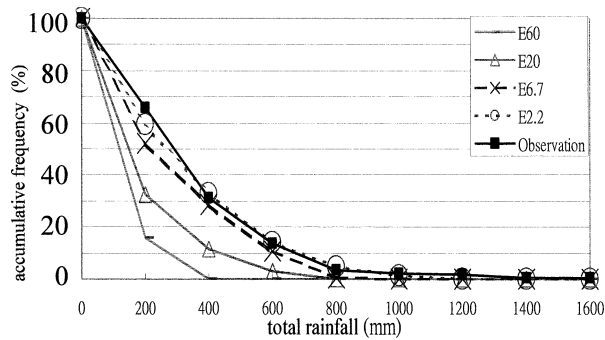


FIG. 7. The cumulative frequency with respect to the 24-h rainfall amount (ending at 0000 UTC 1 Aug 1996) based on data points over the island of Taiwan from E60, E20, E6.7, E2.2, and the rain gauge observation (as shown in Fig. 1b), respectively.

ing of about 2.2 or 6.7 km is the very resolution needed to simulate the rainfall pattern associated with typhoons in the Taiwan area.

To highlight the importance of large-scale, upslope motion in producing heavy rainfall, Fig. 8 shows an east–west vertical cross section of wind (u, w), potential temperature, and RH fields, cutting across Mount A-Li

along 23.3°N at 32 h from E6.7 (which is equal to 0800 UTC 31 July, the time when the model storm is making landfall at northeastern Taiwan). The potential temperature field shows the presence of mountain waves associated with moist stratified flows over topography (Miglietta and Buzzi 2001). Two-dimensional wind vectors, constructed from the cross section, show a significant westerly wind component throughout the troposphere to the west of the CMR, especially for the airflow below 500 hPa. The westerly wind component varies from about 20 m s⁻¹ near the west coast of Taiwan to 35 m s⁻¹ on the top of the CMR. As the airflow impinges upon the CMR, the entire, nearly saturated layer from the surface to 500 hPa is lifted above the mountains. It then descends to the lee of the CMR, generating subsidence warming and drying in the lower troposphere. The entire troposphere along the cross section, under the influence of the typhoon, has an RH close to 100%, except for the localized drying due to subsidence in the upper troposphere above the mountain (minimum RH of 37%) and the lee of the CMR (minimum RH of 50%). This result is consistent with the observed foehn phenomenon and a mesolow over eastern Taiwan between Hualien and Taitung (Shieh et al. 1997). The horizontal

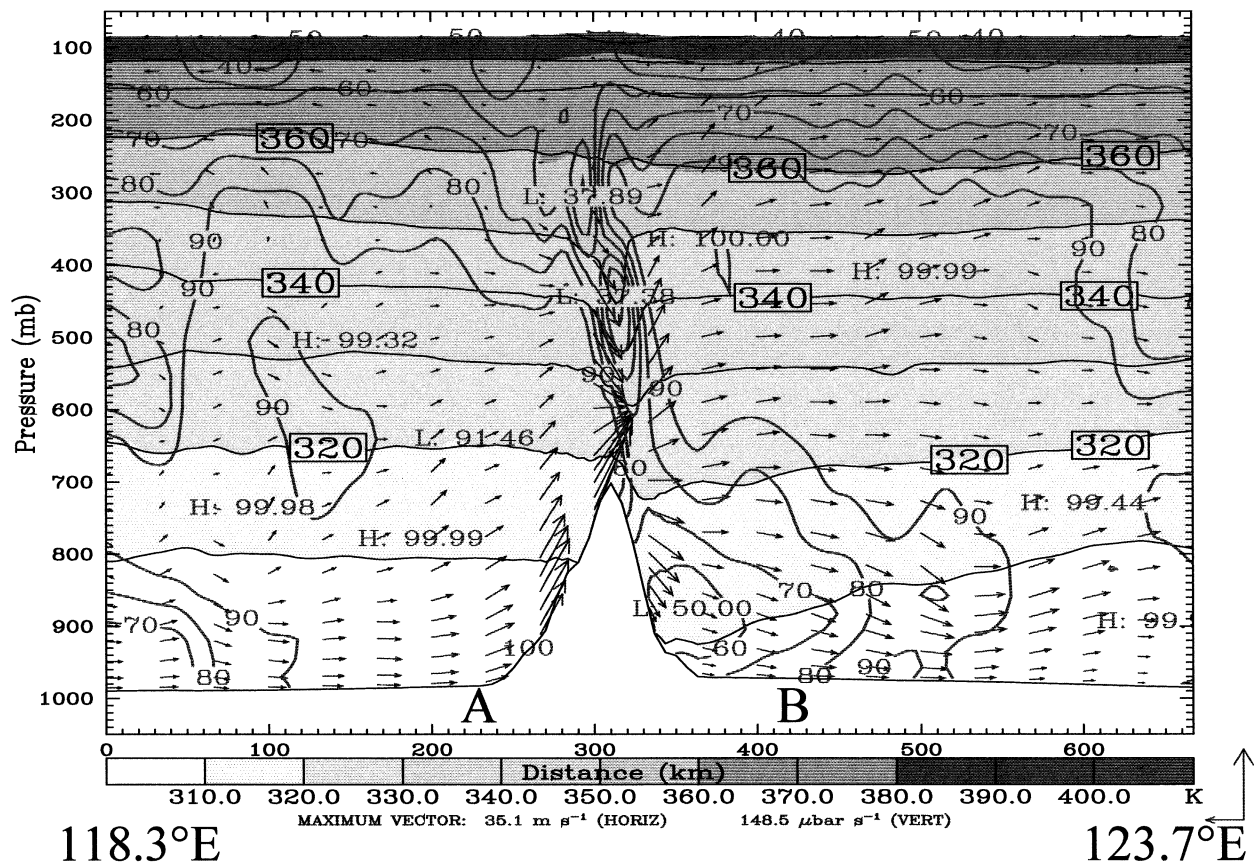


FIG. 8. Zonal cross section (along 23.3°N, and from 118.3° to 123.7°E; see line AB in Fig. 1a) of two-dimensional wind vector (u, w) ($m s^{-1}, \mu b s^{-1}$), temperature (shaded for every 5 K), and relative humidity (contour interval of 5%) fields cutting through Mount A-Li from E6.7 valid at 32-h model integration time (0800 UTC 31 Jul 1996).

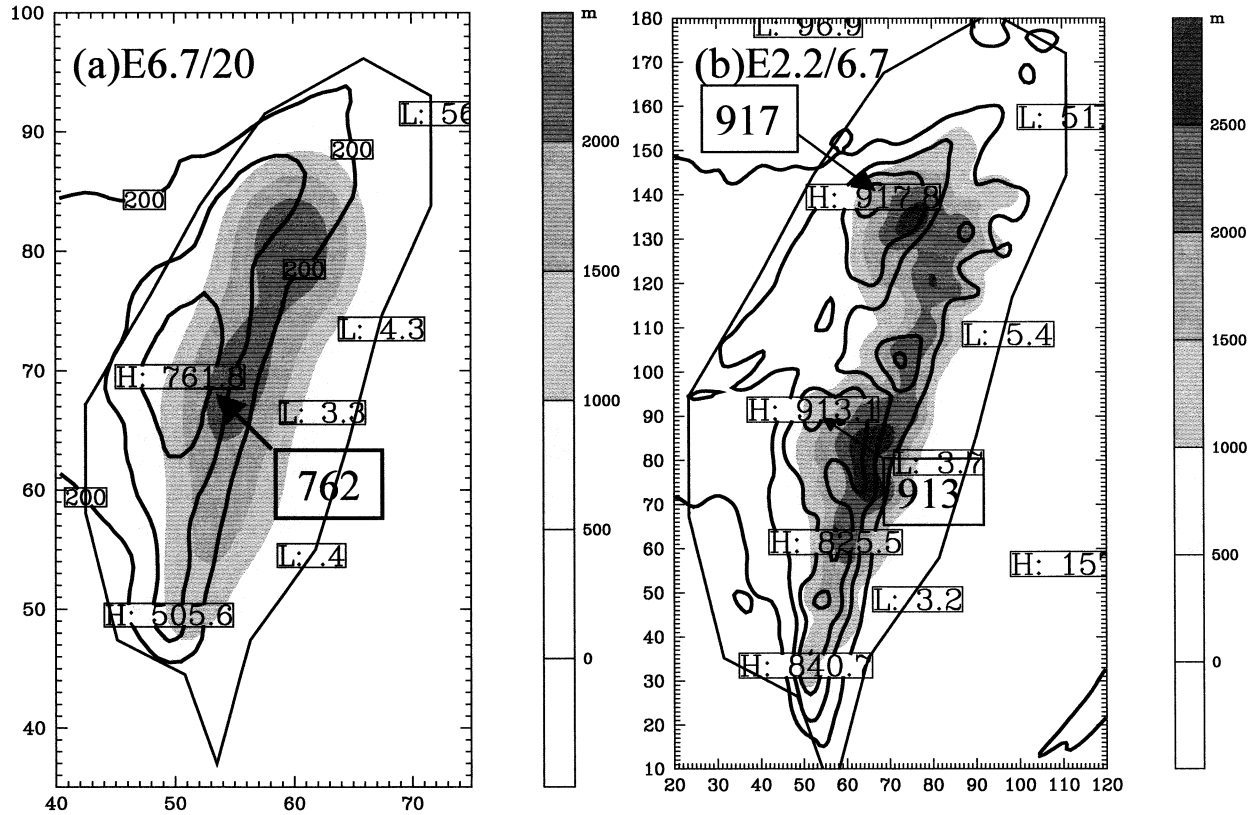


FIG. 9. The 24-h rainfall (contour interval of 200 mm) ending at 0000 UTC 1 Aug 1996 from (a) E6.7/20 and (b) E2.2/6.7. Corresponding model terrains (m) are shown in shading for every 500 m.

wind along the cross section shows that the strong westerly wind component forces a deep layer of upslope motion, thus producing cloud and rainwater (figures not shown) in a nearly saturated typhoon environment.

(ii) Sensitivity of precipitation prediction to terrain and model initialization

A careful comparison of the model terrain and 24-h accumulated rainfall in all four experiments shows that the rainfall takes place mainly along the western slopes of the CMR. On the other hand, results from experiment E6.7/NT (figures not shown) indicate broader and weaker (reduction by more than 50% in peak value as compared with E6.7) rainfall distribution over Taiwan. For experiments with Taiwan terrain, the maximum rainfall tends to occur immediately to the west of the mountain peaks. Based on this result, the importance of upslope flow in producing the extremely heavy rainfall over the CMR is evident.

As discussed in section 2a (Fig. 3a), E6.7/NB contains a fairly weak initial vortex of Herb, and the vortex maintains this intensity (see Fig. 5) during the integration period. Results from this simulation reveal a track similar to E6.7 (see Fig. 4), though the weak vortex without proper initialization in E6.7/NB starts from a different initial location and wobbles around during the first 18

h. It is found that the maximum rainfall amount near Mount A-Li and Nio-Dray from E6.7/NB was reduced by 16% and 35%, individually. It is obvious that the reduction in rainfall can be attributed to the weaker intensity of Herb, as well as to the weakened upslope wind associated with the weaker outer circulation of Herb in E6.7/NB. The result here also suggests the importance of the accurate representation of the initial typhoon vortex, in rainfall simulation over mesoscale topography. In other words, the rainfall is highly modulated by the interaction between the terrain and the flow field associated with the storm's inner and outer circulation.

(iii) Relative impacts of model grid resolution and topography

It is of interest to discern whether the improvement in the rainfall simulation with higher grid resolution is mainly due to the improvement in resolving the mesoscale storm and environmental structure or to the improvement in describing the model terrain. To clarify the above issue, another experiment, E6.7/20 (E2.2/6.7), is included, which is identical to E6.7 (E2.2), except with model terrain interpolated from E20 (E6.7). As shown in Fig. 9, even though the model grid spacing is 6.7 km (2.2 km) in E6.7/20 (E2.2/6.7), except with a

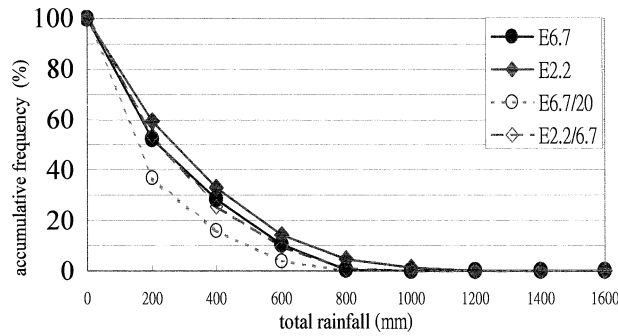


FIG. 10. The cumulative frequency with respect to the 24-h rainfall amount (ending at 0000 UTC 1 Aug 1996) based on data points over the island of Taiwan from E6.7, E2.2, E6.7/20, and E2.2/6.7, respectively.

coarser 20-km (6.7-km) model terrain, the rainfall distribution becomes similar to that of E20 (E6.7) in the rainfall amount at Mount A-Li. In other words, the rainfall maximum near Mount A-Li is reduced from 826 mm (Fig. 6c) in E6.7 to 762 mm (Fig. 9a) in E6.7/20,

likewise from 1199 mm (Fig. 6d) in E2.2 to 913 mm (Fig. 9b) in E2.2/6.7.

The cumulative frequency (Fig. 10) also shows that the overall 24-h rainfall amount is reduced when the terrain resolution is degraded (see the comparison of E2.2 and E2.2/6.7 and the comparison of E6.7 and E6.7/20). Note that when the terrain resolution is reduced to 6.7 km in the simulation with 2.2-km horizontal spacing (i.e., E2.2/6.7), the cumulative frequency (Fig. 10) becomes very similar to the 6.7-km simulation (E6.7), indicating the importance of the terrain effect on the high-resolution rainfall simulation in the Taiwan area.

To understand how the different model and terrain resolutions affect the rainfall simulation, the vertical velocity and the latent heating are averaged over a $0.4^\circ \times 0.4^\circ$ square area (Fig. 1a) at the region of maximum rainfall near Mount A-Li and over a 24-h period (from 0000 UTC 31 July to 0000 UTC 1 August) for the aforementioned experiments. Comparison of the averaged vertical velocity and latent heating profiles (Figs. 11 and 12) shows that both the peak vertical velocity and latent heating are reduced either when the model

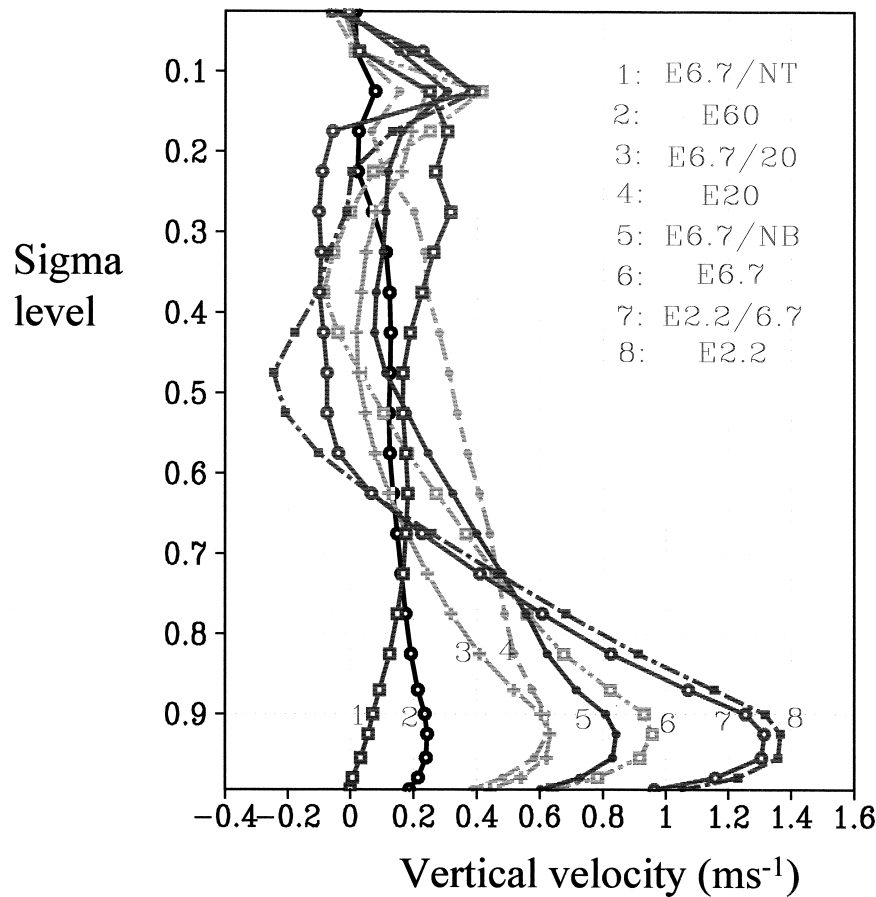


FIG. 11. Vertical profile (in sigma coordinate) of vertical velocity ($m s^{-1}$) averaged over the region ($23.3^\circ\text{--}23.7^\circ\text{N}$, $120.6^\circ\text{--}121.0^\circ\text{E}$) near Mount A-Li (as indicated in Fig. 1) from 0000 UTC 31 Jul to 0000 UTC 1 Aug 1996 for 1) E6.7/NT, 2) E60, 3) E6.7/20, 4) E20, 5) E6.7/NB, 6) E6.7, 7) E2.2/6.7, and 8) E2.2.

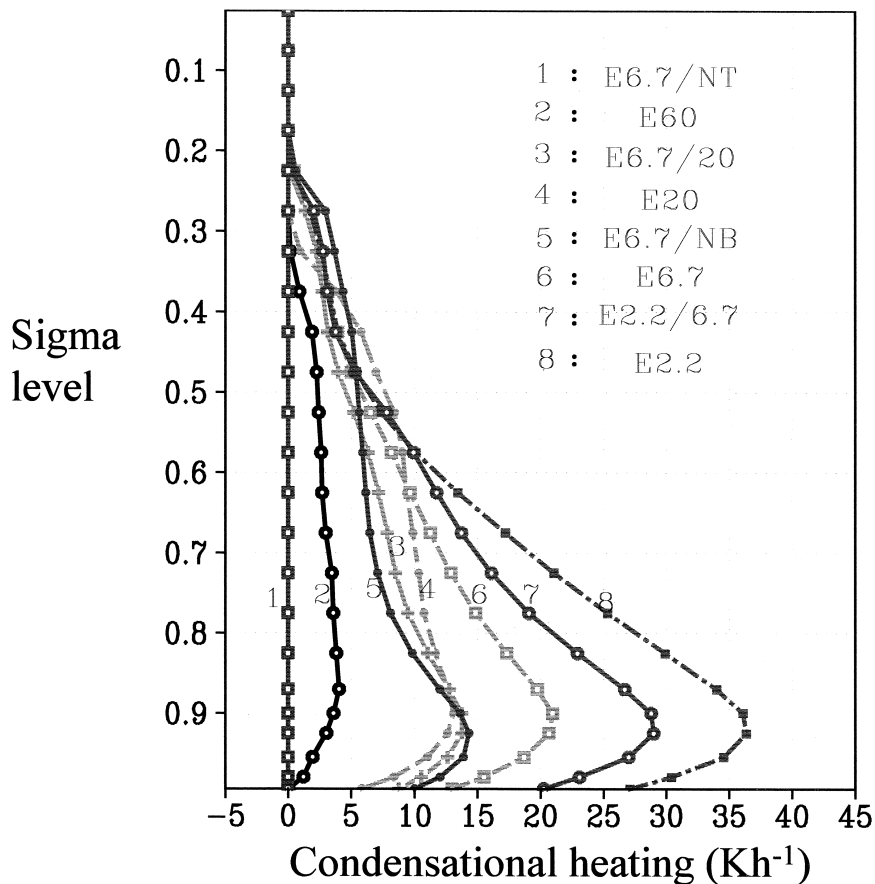


FIG. 12. Same as Fig. 11 but for condensational heating ($K h^{-1}$).

resolution is reduced (see comparison of E60, E20, E6.7, and E2.2) or when the terrain resolution is degraded (see comparison of E6.7 and E6.7/20 and E2.2 and E2.2/6.7). The change in the maximum averaged vertical velocity and condensational heating rate is also consistent with the change of the 24-h accumulated precipitation in all of the above experiments, as shown in Table 2.

In addition, Figs. 11 and 12 show that the simulation with no terrain (E6.7/NT) results in a very different vertical velocity profile and has a much weaker vertical velocity and condensational heating rate when compared with the results in E6.7. Meanwhile, the experiment without extra bogusing (E6.7/NB) has a 15% reduction in the maximum averaged vertical velocity and a 30% reduction in the maximum heating rate, as compared with E6.7. Such a result is also consistent with that, presented in the previous section, of the reduction of

maximum rainfall either when the terrain is removed or when no bogused vortex is implanted during model initialization.

The above results strongly suggest that not only the improvement of model resolution itself but better representation of the model terrain are key factors in producing more realistic rainfall patterns over Taiwan associated with Herb. Note that Figs. 11 and 12 also demonstrate a peculiar vertical velocity and heating profile for this kind of forced lifting over the upslope side of the terrain, by the typhoon's strong outer circulation. To be specific, the forced lifting contains the maximum, upward motion and heating rate in the lower troposphere (at the roughly 0.9 sigma level). The fact that the heating profile occurs at low levels on the windward side of the mountains suggests that this is the location at which the condensation occurs and that it is also likely to be where

TABLE 2. Comparison of the averaged rainfall and w_j near Mount A-Li.

Expt	E60	E20	E6.7	E2.2	E6.7/20	E2.2/6.7
24-h accumulated precipitation (mm) averaged near Mount A-Li	99.0	385.0	565.0	788.0	453.0	666.0
24-h area-averaged w_j ($m s^{-1}$)	0.309	0.414	0.568	0.792	0.467	0.686

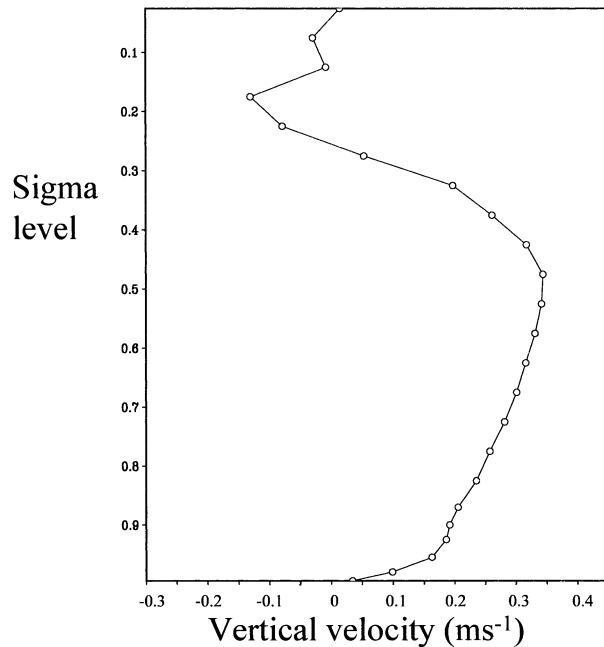


FIG. 13. Vertical profile (in sigma coordinate) of vertical velocity (m s^{-1}) averaged over the inner 100-km radius around the center of Herb for E6.7 at 2200 UTC 30 Jul 1996.

the rain enhancement occurs. The above profile is different from the typical profile that contains maximum values in the middle to upper troposphere within the eyewall region in Herb (Fig. 13; note that, because the inner nest of E2.2 does not cover the offshore storm center, results from E6.7 are used here) or the profile found in a typical oceanic typhoon [e.g., Hurricane Bob (1991) in Figs. 8b and 8d of Wu and Kurihara (1996)].

(iv) *The impact from the topography-induced upward motion*

It has been shown (Lin et al. 2001) that the topography-induced, upward motion plays important roles in the formation of the topographic rainfall. Here, the topography-induced, upward motion w_f has also been calculated as the inner product of the near-surface, horizontal wind vector and the gradient of the topography; that is, $w_f = \mathbf{u}_s \cdot \nabla h$, where \mathbf{u}_s is the wind vector at the lowest model level ($\sigma = 0.995$) and h is the terrain height. As indicated in Fig. 14, the area-averaged w_f near Mount A-Li (as shown by the thickened square box in Fig. 1a) accounts for about 60% of the averaged vertical motion w in the lowest model level during the period from 0200 to 1400 UTC 31 July, when the most intense rainfall is induced in the area. Such results clearly indicate that the terrain plays a major role in inducing the vertical motion.

To indicate the relation among the 24-h rainfall, the terrain height, and the topography-induced vertical velocity w_f , Fig. 15 shows the cross section (cutting through Mount A-Li; line AB as indicated in Fig. 1a)

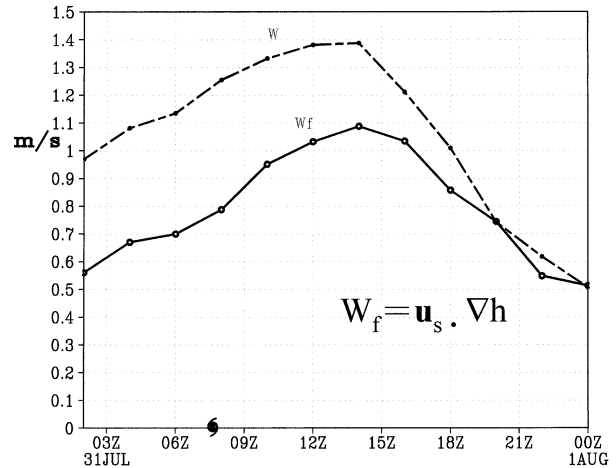


FIG. 14. Time series (from 0200 UTC 31 Jul to 0000 UTC 1 Aug 1996) of the vertical velocity (dashed line, m s^{-1}) at the lowest model level ($\sigma = 0.995$) and the topography-induced vertical motion (w_f , solid line) averaged over the region (23.3° – 23.7°N , 120.6° – 121.0°E) near Mount A-Li (as indicated in Fig. 1). The typhoon symbol indicates the time when the model storm makes landfall.

of the terrain height (shaded), 24-h accumulated rainfall (dashed), and 24-h-averaged w_f (solid) from experiments with different resolutions. It is shown that the 24-h rainfall, terrain height, and w_f all increase as the model resolution is increased. Meanwhile, the rainfall maximum is located at the western side (upwind slope) of the terrain peak, and the distribution of w_f corresponds well to the terrain slope, with its local peak value occurring at a location farther upstream than that associated with the local peak rainfall.

To evaluate quantitatively the relation between the forced vertical motion w_f and the rainfall, the 24-h-averaged w_f and the 24-h-accumulated precipitation, averaged near Mount A-Li, are shown in Table 2. It is found that both the precipitation and w_f decrease when the model resolution (see comparison of E2.2, E6.7, E20, and E60) or the terrain resolution (see comparison of E6.7 and E6.7/20, as well as E2.2 and E2.2/6.7) is reduced. Such positive correlation between precipitation amount and topography-enhanced updrafts agrees with Barros and Lettenmaier (1994) and Lin et al. (2001).

The enhancement percentage of the 24-h-averaged w_f and the 24-h-accumulated precipitation, among experiments with different model or terrain resolutions, is shown in Table 3. The results show that the enhancement percentage of the 24-h-averaged w_f is consistent with that of the 24-h-accumulated precipitation. Comparison C₁ shows that the enhancement percentage of rainfall reaches 288.9% from E60 to E20, because the resolution in E60 is too low to resolve the detailed mountain structure. Therefore, the rainfall amount averaged near Mount A-Li is totally missed. Comparison C₂ (C₃) shows that the enhancement percentage of the rainfall amount increases by 46.8% (39.5%) when both the model and terrain resolutions are increased from 20 (6.7) to

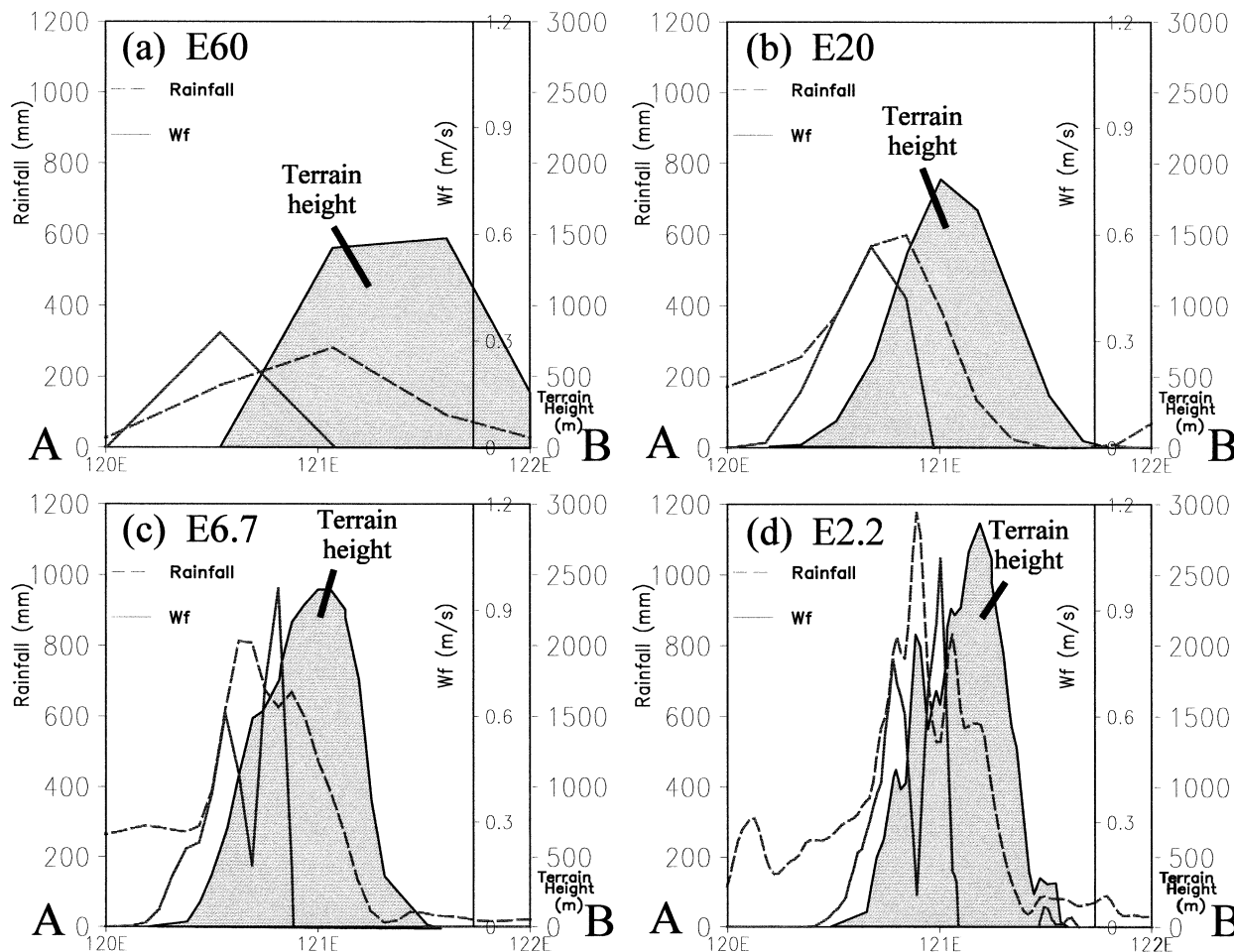


FIG. 15. Zonal cross section (along 23.3°N, and from 120° to 122°E; see line AB in Fig. 1a) of the terrain height (shaded; m), 24-h accumulated rainfall (dashed; mm), and 24-h-averaged w_f (solid; $m s^{-1}$) cutting through Mount A-Li from (a) E60, (b) E20, (c) E6.7, and (d) E2.2.

6.7 (2.2) km. When the model resolution is increased while the terrain resolution remains unchanged, such as in the comparison between E6.7/20 and E20 (E2.2/6.7 and E6.7) in C_4 (C_5), the rainfall enhancement is reduced to 17.7% (17.9%). On the other hand, when only the terrain resolution is improved, as indicated by C_6 (C_7), the rainfall increase is 19.8% (15.5%). The above comparisons obviously indicate that the model and ter-

rain resolutions play nearly equivalent roles in affecting the rainfall amount associated with the topography-enhanced, vertical motion of Herb as it passes Taiwan.

4. Summary

Typhoon Herb made landfall at northeastern Taiwan on 31 July 1996 and was the most damaging tropical

TABLE 3. Enhancement percentage of the rainfall and w_f near Mount A-Li in different experiments.

Comparison	C_1	C_2	C_3	C_4	C_5	C_6	C_7
Definition of each comparison	E20 - E60 E60	E6.7 - E20 E20	E2.2 - E6.7 E6.7	E6.7/20 - E20 E20	E.22/6.7 - E6.7 E6.7	E6.7 - E6.7/20 E6.7	E2.2 - E2.2/6.7 E2.2
Enhancement (%) of the 24-h-averaged rainfall	288.9	46.8	39.5	17.7	17.9	19.8	15.5
Enhancement (%) of the 24-h-averaged w_f ($m s^{-1}$)	34.0	37.2	39.4	12.8	20.8	17.8	13.4

cyclone in the recent history of Taiwan. In this study, we have performed a series of simulation experiments on Typhoon Herb, using MM5 with horizontal grid spacings of 60, 20, 6.7, and 2.2 km. Our primary interest is to examine the ability of the model to simulate the precipitation associated with Typhoon Herb and to assess the impact of horizontal grid resolution and topography on rainfall prediction. The results presented above show that a high-resolution mesoscale model, such as MM5, can be a very useful tool in forecasting the detailed mesoscale precipitation distribution associated with typhoons near Taiwan. We also show that, given a reasonable track prediction, the ability of the model to simulate successfully the observed rainfall is degraded by the reduction of horizontal grid resolution and/or terrain resolution.

An unsurprising finding is that the existence of the CMR plays a key role in substantially increasing the total rainfall amounts associated with Typhoon Herb by lifting the moisture-laden air over the upslope of the mountains. The sensitivity experiments indicate that the model and terrain resolutions play nearly equivalent roles in affecting the rainfall simulation over the mountainous area. Detailed analyses also show an atypical vertical velocity and heating profile, associated with the kind of precipitation growth occurring along the topography, where the maximum upward motion occurs in the lower troposphere. The vertical distribution of the forced upward motion associated with the typhoon circulation over the upslope region is very different from the typical profile, with maximum heating and vertical motion in the middle-to-upper troposphere within the storm eyewall (Wu and Kurihara 1996).

Nevertheless, questions remain unanswered regarding the uncertainty and limitation of the model to the quality of the initial data, the model initialization, and the options of the model physics, such as the microphysics and the boundary layer parameterization (Braun and Tao 2000). For example, our other sensitivity experiments show that the rainfall amount can be sensitive to the microphysical schemes in the model. Such results contain interesting scientific issues of how microphysical processes affect the detailed distributions of hydrometeors and how these distributions, in turn, affect the precipitation amount (especially for simulation at high horizontal resolution and over complicated terrain). Full attention will be paid to addressing the issues of microphysics in the second part of this paper.

Meanwhile, as indicated in Wu and Kuo (1999), it remains unanswered why Herb produced such exceptionally heavy rainfall. Experiments for typhoons of different intensities, sizes, and humidities, as well as at different locations and with various movement speeds will be conducted to obtain better understanding of the factors leading to such extreme rainfall. These results will also be shown in the follow-up paper.

Because the rainfall distribution for typhoons affecting Taiwan is highly modulated by the topography of

Taiwan (Wu and Kuo 1999), the mesoscale precipitation distribution associated with a landfalling typhoon in Taiwan remains a major challenge for numerical models, given the uncertainty in simulating the landfall location and typhoon intensity. Therefore, additional research is required to assess the potential of high-resolution mesoscale models, which incorporate improved radar or satellite data through advanced data assimilation techniques (e.g., Guo et al. 2000; Zou and Xiao 2000), in predicting detailed wind and rainfall distributions for typhoons affecting Taiwan.

Acknowledgments. Helpful discussions with Drs. Yuh-Lang Lin, Yuqing Wang, Da-Lin Zhang, and Wei-Kuo Tao are appreciated. We also thank Dr. Frank Marks and the anonymous reviewers for helpful comments. This work is partially supported through the National Science Council of Taiwan by Grants NSC88-2111-M-002-004-AP1 and NSC89-2111-M-002-020-AP1.

REFERENCES

- Barros, A. P., and D. P. Lettenmaier, 1994: Dynamic modeling of orographically induced precipitation. *Rev. Geophys.*, **32**, 265–284.
- Bender, M. A., R. E. Tuleya, and Y. Kurihara, 1987: A numerical study of the effect of island terrain on tropical cyclones. *Mon. Wea. Rev.*, **115**, 130–155.
- Betts, A. K., and M. J. Miller, 1986: A new convective adjustment scheme. Part II: Single column tests using GATE wave, BOMEX, ATEX and Arctic air-mass data sets. *Quart. J. Roy. Meteor. Soc.*, **112**, 693–709.
- Braun, S. A., and W.-K. Tao, 2000: Sensitivity of high-resolution simulations of Hurricane Bob (1991) to planetary boundary layer parameterizations. *Mon. Wea. Rev.*, **128**, 3941–3961.
- Dudhia, J., 1989: Numerical study of convection observed during the Winter Monsoon Experiment using a mesoscale two-dimensional model. *J. Atmos. Sci.*, **46**, 3077–3107.
- , 1993: A nonhydrostatic version of the Penn State–NCAR Mesoscale Model: Validation tests and simulation of an Atlantic cyclone and cold front. *Mon. Wea. Rev.*, **121**, 1493–1513.
- Emanuel, K., and Coauthors, 1995: Report of the First Prospectus Development Team of the U.S. Weather Research Program to NOAA and the NSF. *Bull. Amer. Meteor. Soc.*, **76**, 1194–1208.
- Farfan, L. M., and J. A. Zehnder, 2001: An analysis of the landfall of Hurricane Nora (1997). *Mon. Wea. Rev.*, **129**, 2073–2088.
- Grell, G. A., J. Dudhia, and D. R. Stauffer, 1994: A description of the fifth generation Penn State/NCAR Mesoscale Model (MM5). NCAR Tech. Note NCAR/TN-398+STR, 138 pp.
- Guo, Y.-R., Y.-H. Kuo, J. Dudhia, and D. Parsons, 2000: Four-dimensional data assimilation of heterogeneous mesoscale observations for a strong convective case. *Mon. Wea. Rev.*, **128**, 619–643.
- Kuo, Y.-H., and W. Wang, 1997: Rainfall prediction of Typhoon Herb with a mesoscale model. Preprints, *Workshop on Typhoon Research in the Taiwan Area*, Boulder, CO, National Science Council, 35–45.
- Kurihara, Y., M. A. Bender, R. E. Tuleya, and R. J. Ross, 1995: Improvements in the GFDL hurricane prediction system. *Mon. Wea. Rev.*, **123**, 2791–2801.
- , —, —, and —, 1998: The GFDL hurricane prediction system and its performance in the 1995 hurricane season. *Mon. Wea. Rev.*, **126**, 1306–1322.
- Lin, Y.-L., 1993: Orographic effects on airflow and mesoscale weather systems over Taiwan. *Terr. Atmos. Oceanic Sci.*, **4**, 381–420.
- , S. Chiao, T.-A. Wang, M. L. Kaplan, and R. P. Weglarz, 2001:

- Some common ingredients for heavy orographic rainfall. *Wea. Forecasting*, **16**, 633–660.
- Liu, Y., D.-L. Zhang, and M. K. Yau, 1997: A multiscale numerical study of Hurricane Andrew (1992). Part I: Explicit simulation and verification. *Mon. Wea. Rev.*, **125**, 3073–3093.
- , —, and —, 1999: A multiscale numerical study of Hurricane Andrew (1992). Part II: Kinematics and inner-core structures. *Mon. Wea. Rev.*, **127**, 2597–2616.
- Marks, F. D., and Coauthors, 1998: Landfalling tropical cyclones: Forecast problems and associated research opportunities. *Bull. Amer. Meteor. Soc.*, **79**, 305–323.
- Miglietta, M. M., and A. Buzzi, 2001: A numerical study of moist stratified flows over isolated topography. *Tellus*, **53A**, 481–499.
- Reisner, J., R. M. Rasmussen, and R. T. Bruintjes, 1998: Explicit forecasting of supercooled liquid water in winter storms using the MM5 mesoscale model. *Quart. J. Roy. Meteor. Soc.*, **124**, 1071–1107.
- Shieh, S.-L., S.-T. Wang, M.-D. Cheng, and T.-C. Yeh, 1997: User's guide for typhoon forecasting in the Taiwan area (in Chinese). Central Weather Bureau Research Rep. CWB85-1M-01, 381 pp. [Available from S.-T. Wang, Central Weather Bureau, 64, Kung-Yuan Rd., Taipei 100, Taiwan.]
- Wang, S.-T., 1980: Prediction of the behavior and intensity of typhoons in Taiwan and its vicinity (in Chinese). Research Rep. 018, NSC-67M-0202-01 (01), National Science Council, 100 pp. [Available from S.-T. Wang, Central Weather Bureau, 64, Kung-Yuan Rd., Taipei 100, Taiwan.]
- , 1989: Track, intensity, structure, wind and precipitation characteristics of typhoons affecting Taiwan (in Chinese). Disaster Mitigation Research Rep. 80-73, NSC 80-04140-P052-02B, National Science Council, 285 pp. [Available from S.-T. Wang, Central Weather Bureau, 64, Kung-Yuan Rd., Taipei 100, Taiwan.]
- Wang, Y., 2001: An explicit simulation of tropical cyclones with a triply nested movable mesh primitive equation model: TCM3. Part I: Model description and control experiment. *Mon. Wea. Rev.*, **129**, 1370–1394.
- Wu, C.-C., 2001: Numerical simulation of Typhoon Gladys (1994) and its interaction with Taiwan terrain using the GFDL hurricane model. *Mon. Wea. Rev.*, **129**, 1533–1549.
- , and Y. Kurihara, 1996: A numerical study of the feedback mechanisms of hurricane–environment interaction on hurricane movement from the potential vorticity perspective. *J. Atmos. Sci.*, **53**, 2264–2282.
- , and Y.-H. Kuo, 1999: Typhoons affecting Taiwan—current understanding and future challenges. *Bull. Amer. Meteor. Soc.*, **80**, 67–80.
- , and W.-P. Huang, 2000: Numerical simulation of Typhoon Flo (1990) using a non-hydrostatic mesoscale model: The impact of initial data and initialization schemes (in Chinese with English abstract). *Atmos. Sci.*, **28**, 293–316.
- , M. Bender, and Y. Kurihara, 2000: Typhoon forecasts with the GFDL hurricane model: Forecast skill and comparison of predictions using AVN and NOGAPS global analyses. *J. Meteor. Soc. Japan*, **78**, 777–788.
- Yeh, T.-C., and R. L. Elsberry, 1993a: Interaction of typhoons with the Taiwan orography. Part I: Upstream track deflections. *Mon. Wea. Rev.*, **121**, 3193–3212.
- , and —, 1993b: Interaction of typhoons with the Taiwan orography. Part II: Continuous and discontinuous tracks across the island. *Mon. Wea. Rev.*, **121**, 3213–3233.
- Zou, X., and Q. Xiao, 2000: Studies on the initialization and simulation of a mature hurricane using a variational bogus data assimilation scheme. *J. Atmos. Sci.*, **57**, 836–860.